NDT&E International 62 (2014) 85–92

Contents lists available at ScienceDirect

NDT&E International

journal homepage: www.elsevier.com/locate/ndteint

Investigation of thermal imaging sampling frequency for eddy current pulsed thermography

Jia Liu [a], Gui Yun Tian [a,b,*], Bin Gao [a,b,*], WenWei Ren [a], Jin Song Meng [a]

[a] School of Automation, University of Electronic Science and Technology of China, Chengdu, China
[b] School of Electrical and Electronic Engineering, Newcastle University, UK

ARTICLE INFO

Article history:
Received 29 September 2013
Received in revised form
22 November 2013
Accepted 25 November 2013
Available online 11 December 2013

Keywords:
Eddy Current Pulsed Thermography (ECPT)
Sampling rate
Source separation
Non-Destructive Testing and Evaluation (NDT&E)
Quantitative NDE

ABSTRACT

Eddy Current Pulsed Thermography (ECPT) is an integrative Non-Destructive Testing and Evaluation (NDT&E) technique that has been applied for defect and material characterization of conductive material and components. Thermal transient images provide rich information for decision making. However, high sampling rates of a thermal camera creates high cost and will generate a large of amount of data which is difficult for remote monitoring in terms of computational efficiency and data communication. This paper investigates the impact of thermal image sampling rates versus feature extraction for defect characterization. After introduction of Eddy Current Pulsed Thermography (ECPT), different sampling rates of thermal images are applied for different characterization. Based on the feature robustness versus different sampling rates, appropriate sampling rates are reported. The impact of using high end and low end thermal cameras for ECPT non-destructive evaluation are discussed.

1. Introduction

Ultrasonic [1] testing, X-ray [2], eddy current [3], acoustic emission [4], microwave [5], computer tomography (CT) [6] and thermography have been widely used in Non-Destructive Testing and Evaluation (NDT&E). The use of thermography based defect detection [7–9] has the potential for accurate non-contact inspection of a large area within a short time as well as large standoff distances [10]. In addition, thermography is applicable to a wide range of materials, including glass fiber, carbon fiber composites, and metallic materials [11–14]. However, current thermography based detection methods are mostly applied to samples in the lab rather than to in-situ structures, and the high heat absorption rate of the surface and specific excitation techniques are required for different applications [10]. Since different NDT&E techniques have different characteristics, the integration of different NDT&E techniques to achieve high defect detection resolution is required.

Combining both eddy current and thermography techniques enables defects to be detected with its own advantages [15–22]. Flash and laser thermography mainly introduce heat at the surface, whereas the technique known as eddy current pulsed thermography (ECPT) or pulsed eddy current (PEC) thermography applies high current electromagnetic pulse to the conductive material under inspection. The heat is not limited to the sample surface, rather it can reach a certain depth, which is governed by the skin depth of eddy current. Furthermore, thermosonics and ECPT focus the heat on the defect due to friction or eddy current distortion, which increase the temperature contrast between the defective region and defect-free areas. Flash, laser thermography and ECPT are non-contact methods, whilst a couplant is normally required for thermosonics. From point of view of inspection depth, flash thermography is adaptable by changing the lock-in frequency for defects at different depths. From adaptability in terms of defect orientation, ECPT can enhance specific excitation direction to optimize the directional evaluation along the defect orientation which is more effective for geometrically complex components and showed more crack indication. Furthermore, ECPT allows area imaging of defects without scanning and enables to detect both magnetic and non-magnetic metals with rich frequency components fabricated from excitation power. ECPT has been applied in a number of previous studies including an investigation into the temperature distribution around cracks with different penetration depths in metallic materials [23] as well as research discussing the potential for small defect detection in components of complex geometry estimating the probability of detection (POD) of fatigue cracks in steel [24]. Another study has examined detection of multiple cracks from rolling contact fatigue in rail tracks in a single measurement [25]. Quantitative NDE (QNDE) at a pixel level has been reported in previous PEC work and can help derive multiple

* Corresponding authors at: School of Automation, University of Electronic Science and Technology of China, Chengdu, China.
E-mail addresses: g.y.tian@ncl.ac.uk (G.Y. Tian), bin_gao@uestc.edu.cn, bingao831210@gmail.com (B. Gao).

0963-8695/$ - see front matter © 2013 Elsevier Ltd. All rights reserved.
http://dx.doi.org/10.1016/j.ndteint.2013.11.009

properties of materials [18] as well as defect quantification using ECPT [26–28]. The heating distribution on resultant surfaces from direct EC heating and diffused heating can be obtained easily with a thermal camera [29]. Both Principal Component Analysis (PCA) [28] and Independent Component Analysis (ICA) [30-32] could improve the flaw detectivity of thermography, and characterized the surface flaw depth.

As mentioned above, in order to achieve better detect resolution, high sampling acquisition rate of the IR camera is demanded. A sampling frequency of 383 Hz is commonly used to sample thermal image sequences for high fidelity defect detection [33,34]. However, high sampling rate thermal cameras are high in cost and require significant data processing, which is difficult for remote monitoring in term of computational efficiency and data communication. Specifically, a thermal camera with a 320×256 array of 1.5–5 μm InSb detectors has a maximum 383 Hz frame rate [35] where nearly fifteen million data points are produced within 0.5 s, which will lead large redundancy in the post processing. Therefore, the research on down sampled thermal data and feature extraction is necessary to better understand and select proper sampling IR camera for ECPT based NDT&E. In this paper, the automatic different down sampled IR data is generated and single channel blind source separation is used for feature extraction and defect detection on those different down sampled IR data. As RMSE [36] (root mean square error) and SSIM [37,38] (structural similarity index measurement) are very sensitive to small

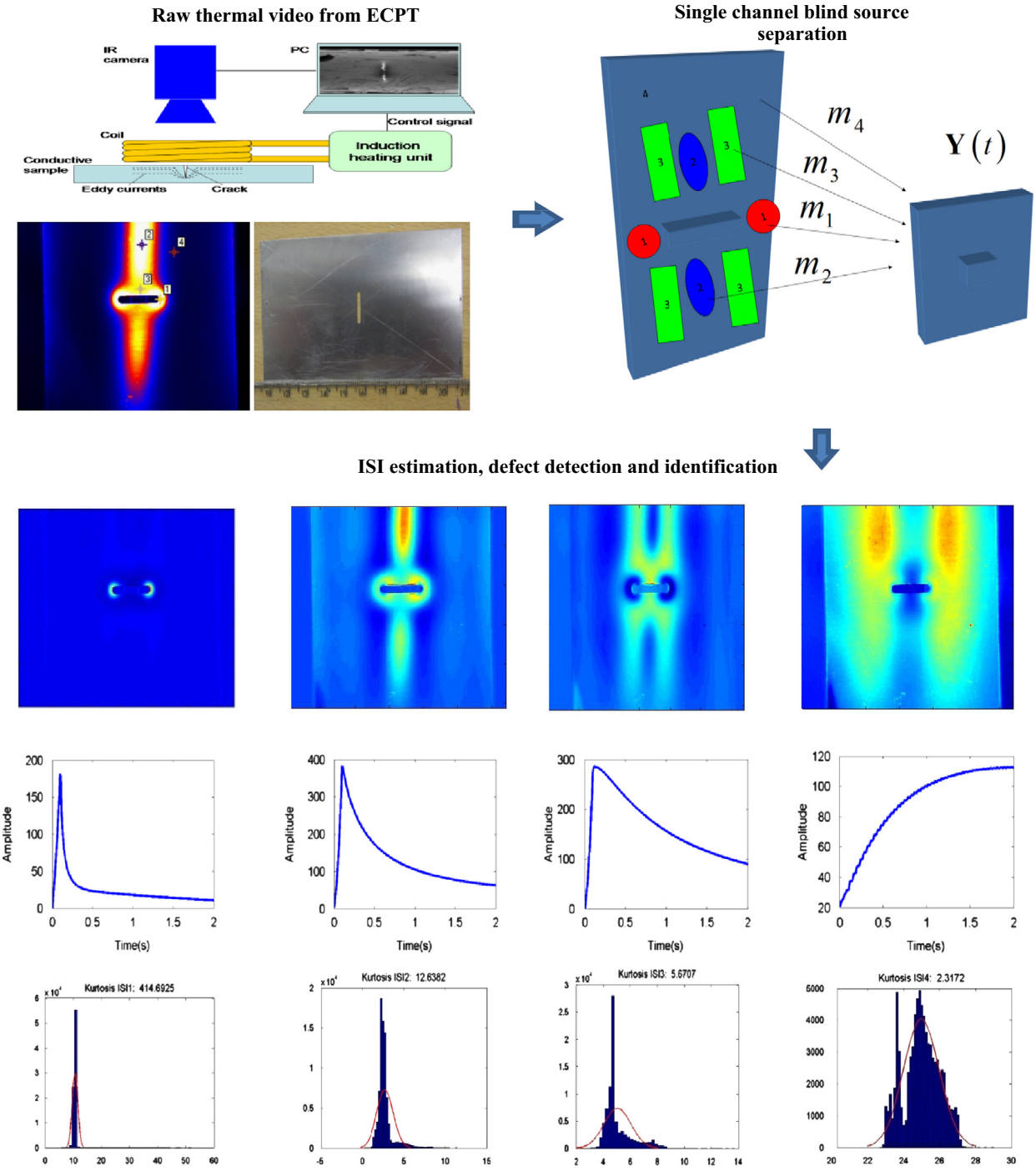

Fig. 1. Flow diagram of blind source separation method for ECPT defect detection.

errors for a set of measurements, they are used to compare the difference between the feature extraction results on high and down sampled IR data, respectively. Quantitative analyses are then applied to understand the effects of ECPT on defects with different sampling rates.

The rest of this paper has been organized as follows. Firstly, specimens, feature extraction and the method of comparing the material feature with different sampling rates are introduced in Section 2. The experimental study and numerical quantitative analysis of material features with different sampling rate are provided in Section 3. Finally, conclusions and further work are outlined in Section 4.

2. Methodology

After review of the ECPT system and its feature extraction, specific feature extraction via different IR imaging sampling frequencies will be investigated.

2.1. ECPT and ICA for feature extraction

In this paper, a guidance how different thermal image sampling rates (From high to low cost IR Camera) affect the defect detection by using ECPT system is investigated. Because it is difficult to directly manually select thermal image to detect defects, therefore we use our previous published methods named as single channel blind source separation (SCBSS) [32,39] for defect detection. During the ECPT testing, when eddy current encounters a discontinuity (e.g. a slot or notch), they are forced to divert leading to assembly areas of increased and decreased eddy current density as well as the resultant hot and cool area due to Joule heating. Hot spots are observed around the slot tips and the cool areas are located at both sides of the slot. In the cooling phase, heat is diffused from a high temperature area to low temperature area, and reduces the contrast. In addition, the area which is located far away from excitation coil will have continually rising temperature because of heat diffusion. These different areas can be considered as the independent regions which share the similar transient responses in the sample. The infrared camera functioned as a temperature spatial image signal recorder along with time flowing. In this case, as only one camera exists, this refers to 'single channel'. In addition, the camera actually records the mixed image signal corresponding to the signal image from the independent regions at each time point. This can be seen in Fig. 1. Therefore, the task of using blind source separation method is to separate the observed signal image sequence into independent signal images (ISI) as well as their corresponding transient response and automatically identify the one which relates to defect. Specifically, in Fig. 1 bottom panel, ISI 1 highlights the singular pattern around the crack tips. In IC 2, the heat generation rate in the heating period and temperature gradient at the early stage of cooling phase is moderate. Consequently, a moderate rising and cooling rate in the heating phase and cooling phase is generated. In IC 3, the slowest falling rate appears. This position (at the side of the slot) is surrounded by high temperature areas (slot tips and the area underneath the coil), the heat continually penetrates from the surrounding area to this position. In IC 4 the temperature decreases from top to bottom with lift-off increasing and no inductive heating involved. Thus, the heat diffusion from the high temperature areas dominates the thermo pattern and a continuous temperature rising is observed. In this paper, this method is used for processing the different sampled IR mixed image sequences and feature robustness versus different sampling rates, appropriate sampling rates are reported.

In order to find an appropriate sample rate, SSIM and RMSE is used to compare the extracted ISIs with different sampling rates. RMSE (root-mean-square error) is known as the standard error. As RMSE is very sensitive to small errors for a set of measurements, the standard error can be a good indicator of measurement precision. This is one of the primary reasons why the standard error is widely used in the engineering field. RMSE can be defined as $\sigma = \sqrt{((\sum d_i \hat{2})/n)}$, where n is the number of measurements and d_i is the deviation between a measurement and the mean value. Structural similarity (SSIM) index measurement system is a new index of Image similarity measure. The structural similarity theory presents that natural image signals are highly structured, the structure has a very strong correlation between pixels, especially the spatial correlation of pixel is closest. The structural similarity theory contains important information of an object structure in a visual scene.

As mentioned above, the SCBSS of defect detection using ECPT is summarized in Fig. 1. In comparison, firstly, the different down sampled IR data is gained from the ECPT system. Secondly, the ISIs with associated transient patterns are estimated using SCBSS method. Finally, the comparison of ISIs and transient patterns obtained by SCBSS on different sampling rate is analyzed.

In this article, RMSE is used to calculate the errors of transient responses after reducing performance of the thermal camera. SSIM is used to compare the similarity of thermal images with different frequencies. When the value of structural similarity index (SSIM) is greater, the two images are more similar. The maximum value of this index is 1. In order to show the difference value of two images, the difference between two thermal images with high and low frequency is calculated by subtracting the index value of the two thermal images from the maximum value of this index (the value is 1). Thus, the impact of extracting material features is explored after changing thermal imager performance.

3. Results and discussion

3.1. Sample preparation and experiments setup

A steel sample ($0.24 \times 45 \times 100\ mm^3$) with a slot of 10 mm length, 2 mm width is prepared (Fig. 2a). A 100 ms heating duration is selected for inspection, which is long enough to elicit an observable heat pattern.

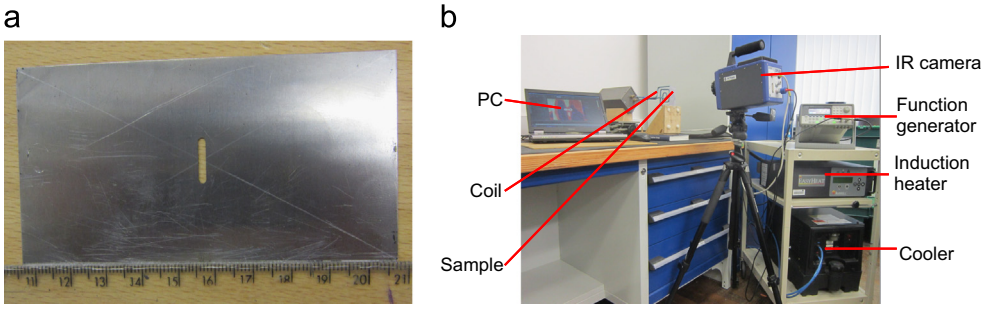

Fig. 2. (a) steel sample with slot and (b) experiment set-up.

The experimental set-up is shown in Fig. 2(a). An Easyheat 224 from Cheltenham Induction Heating is used for coil excitation. The Easyheat has a maximum excitation power of 2.4 kW, a maximum current of 400 A_{rms} and an excitation frequency range of 150–400 kHz (380 A_{rms} and 256 kHz are used in this study). The system has a quoted rise time (from the start of the heating period to full power) of 5 ms, which was verified experimentally. Water cooling of the coil is implemented to counteract direct heating of the coil.

The IR camera, SC7500 is a Stirling cooled camera with a 320×256 array of 1.5–5 μm InSb detectors. This camera has a sensitivity of < 20 mK and a maximum full frame rate of 383 Hz, with the option to increase frame rate with windowing of the image. A rectangular coil is constructed to apply directional excitation. This coil is made of 6.35 mm high conductivity hollow copper tube. In the experiment, only one edge of the rectangular coil is used to stimulate eddy current to the underneath sample. In this study, the frame rate is 383 Hz, and 2 s videos are recorded in the experiments.

3.2. ISI defect detection comparison of using high and low sampled IR data

In this section, both high and low sampled IR data will be tested by using SCBSSS. In order to investigate the effects on the performance of feature extraction of high and low sampled IR data, three comparison cases have been developed:

(i) The ISI comparison associated with spatial resolution of a defect region based on different down sampled IR data will be verified.
(ii) The ISI comparison associated with spatial resolution of other non-defect regions based on different down sampled IR data will be verified.
(iii) The comparison of estimated transient response based on different down sampled IR data will be verified.

From those comparison cases, the impact of extracting material features is explored after changing thermal imager performance. In this experiment, the IR camera, SC7500 with sampling rate of 383 Hz is considered as a reference high-end camera, and the down sampled IR data is then obtained by progressively decreasing the reference IR camera from 383 Hz to 3 Hz (shown in Fig. 3).

From Fig. 3, in order to analyze the different performance of high and low end ECPT system for defect detection, ISI 1 which characterizes defects as shown in Fig. 1 is analyzed.

From Fig. 3(a)–(c), the ISI 1 is taken to analyze defect detection intuitively where it highlights the singular pattern around the crack tips, the intensity degree of highlighting the probe tip shows

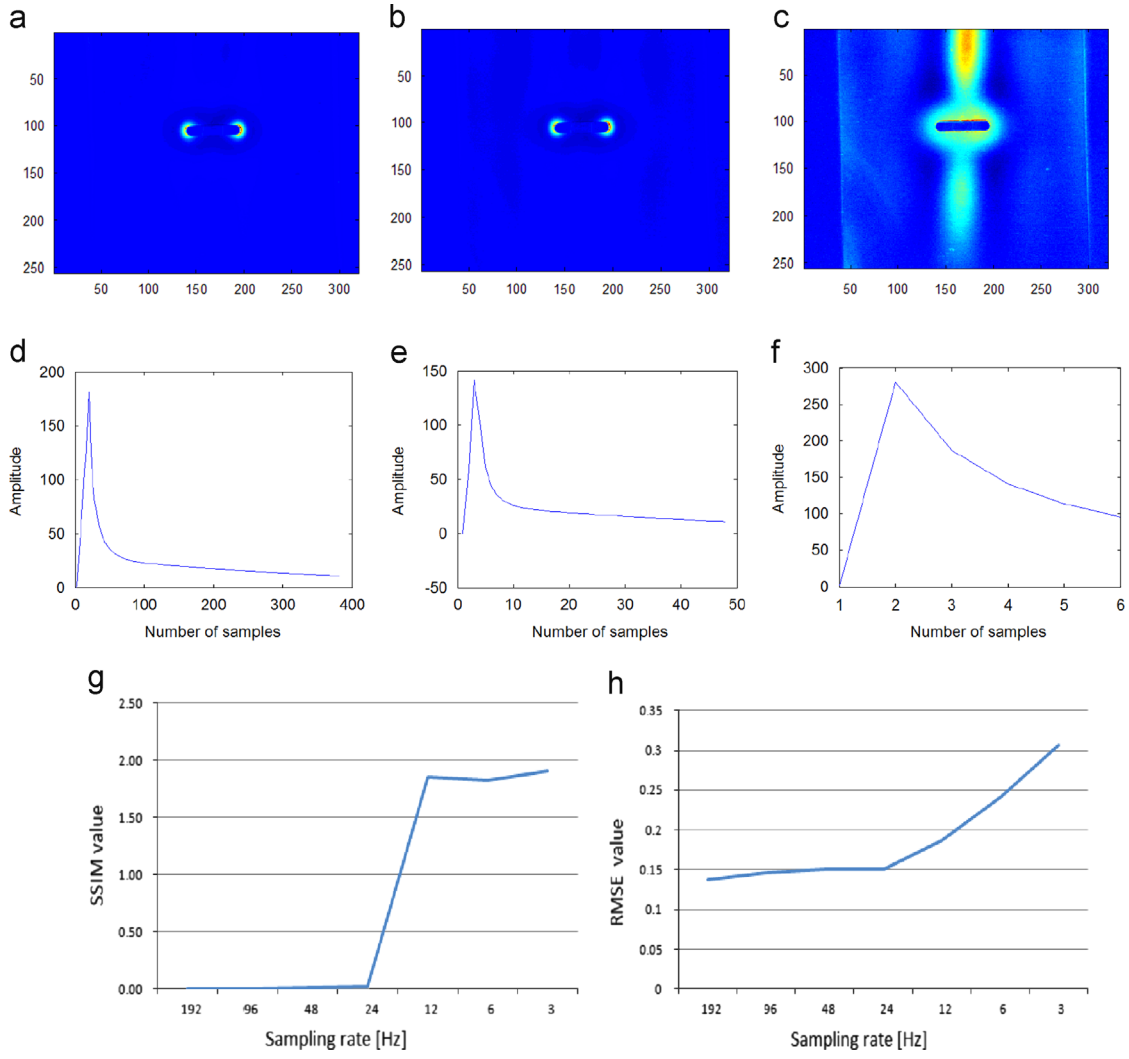

Fig. 3. Comparison of the defect feature with different sampling rate. The ISI 1: (a) the sampling rate is 191, (b) the sampling rate is 24, and (c) the sampling rate is 3. The estimation of transient features: (d) the sampling rate is 191, (e) the sampling rate is 24, and (f) the sampling rate is 3. (g) The SSIM difference of extracted ISI of defect region corresponds to different sampled IR data; (h) the RMSE difference of estimated transient features corresponds to different sampled IR data

defect detection performance. Although the extraction process is based on different sampled IR data, the location of the defect can be still observed except when a down sample rate of 3 Hz is reached. When range of sampling rate is from 24 Hz to 192 Hz, the performance of defect detection does not significantly vary as shown in Fig. 3(a) and (b). However, when the sampling rate is reduced to 3 Hz the intensity degree of highlighting the probe drops and many confounding factors appear to affect defect detection as shown in Fig. 3(c). From Fig. 3(g), it can be seen that the errors increase when the sampling rate decreases. Within the range of 24–192 Hz, the mean of SSIM value is 0.0075 and variance 0.0065. Within the range of 3 Hz up to 12 Hz, the mean of SSIM value is 1.8627 and variance gives 0.0370. Therefore, when the sampling rate is reduced from 192 to 24 Hz, the errors vary small with variance of 0.0065. When the down sampled rate is lower than 12 Hz, the error increases sharply with value of 0.0370. This illustrates the ability of defect detection by using SCBSS method is acceptable when IR data acquisition rate should be higher than 24 Hz.

From Fig. 3(d)–(f), the estimated transient responses associated with independent component 1 are taken to analyze thermal response process of defect detection. Although the frequency changes, thermal response process of independent component 1 still increases firstly and then decreases. However, the values of the thermal response and the coherence of the curve change. As shown in Fig. 3(d) and (e), when the sample rate is ranging from 191 to 24 Hz, the performance of transient responses does not change obviously. However, when the frequency is 3 Hz, the coherence of the curve changes obviously and the curve lost too many information to analyze the process of transient responses as shown in Fig. 3(f). From Fig. 3(h), RMSE is used to characterize the quantitative analysis of the transient responses performance. As shown in Fig. 3(f), the error of the thermal image increases with the frequency reduction. Similarly, when a multiple of the reduction does not exceed 16, the difference between each is little. When the multiple is higher than 16, the error is significantly increased. Within the range of 24-Hz up to 192 Hz, the mean of RMSE value is 0.146 and variance gives 0.138. Within the range of 3 Hz up to 12 Hz, the mean of RMSE value is 0.245 and variance gives 0.352. Therefore, in order to accurately display transient responses, IR data acquisition rate is required to be higher than 24 Hz. Based on the comparison using both ISI and transient

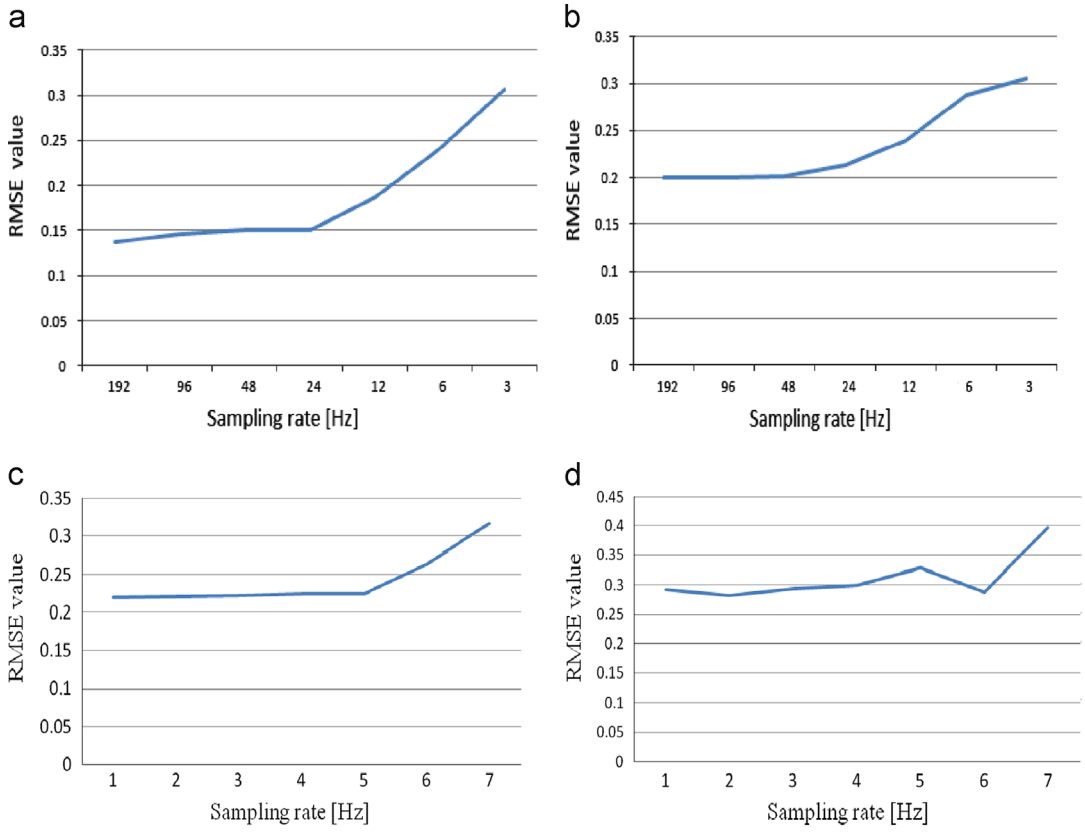

Fig. 4. The error of estimation transient features with different sampling rate: (a) independent component 1, (b) independent component 2, (c) independent component 3, and (d) independent component 4.

Table 1
The comparison of estimated transient patterns obtained by SCBSS on different sampled IR data.

	The critical sampling rate (Tsc)	The mean of RMSE value (Ts > Tsc)	The variance of RMSE value (Ts > Tsc)	The mean of RMSE value (Ts < Tsc)	The variance of RMSE value (Ts < Tsc)
Transient pattern 1	24	0.146	0.138	0.245	0.352
Transient pattern 2	48	0.2	0.00088129	0.2613	0.0367
Transient pattern 3	12	0.222	0.0019	0.2903	0.2896
Transient pattern 4	24	0.2923	0.0062	0.3379	0.0452

Note: Ts means the sampling rate, and Tsc means the critical sampling rate.

feature, it can be concluded that, with accepted range of defect detection resolution by using blind source separation method required at least 24 Hz sampling rate IR camera.

3.3. All ISI comparison of using high and low sampled IR data

As shown in Fig. 4, in order to analyze different performance of high and low end ECPT system for transient responses, four independent components which contain all information of thermal images are analyzed. It can be seen in Fig. 4 and Table 1, as the sampling rate become lower, the errors of the transient responses increase. There exits critical sampling point in analyzing four transient patterns. When the sampling rate is higher than the critical sampling rate, the error between referenced ISI (which are processed by using high end camera 383 Hz) with down sampled IR camera (e.g. 192, 96, etc.) is small. When the sampling rate is lower than the critical sampling rate, the errors increase significantly. In transient pattern 1, the mean of RMSE value is 0.146 and variance gives 0.138 within the range of 24 Hz up to192 Hz, and the mean of RMSE value is 0.245 and variance gives 0.352 within the range of 3 Hz up to 12 Hz. For transient pattern 2, the mean of RMSE value is 0.200 and variance gives 8.8129e−004 within the range of 48–192 Hz, and the mean of RMSE value is 0.2613 and variance gives 0.0367 within the range of 24–3 Hz. For transient pattern 3, the mean of RMSE value is 0.2220 and variance gives 0.0019 within the range of 12–192, and the mean of RMSE value is 0.2903 and variance gives 0.2896 within the range of 6–3 Hz. For transient pattern 4, the mean of RMSE value is 0.2923 and variance gives 0.0062 within the range of 24–192 Hz, and the mean of RMSE value is 0.3379 and variance gives 0.0452 within the range of 12–3 Hz. Therefore, for transient patterns 1 and 4, the critical sampling rate is 24 Hz as shown in Fig. 4(a) and (d). For transient pattern 2, the critical sampling rate is 48 Hz as shown in Fig. 4(b). For transient pattern 3, the critical sampling rate is 12 Hz as shown in Fig. 4(c). The estimation of transient feature is directly used for identifying transient patterns which correspond to defect region. Therefore, in order to ensure the accuracy of the estimation of transient features, sampling rate is required to be higher than 48 Hz.

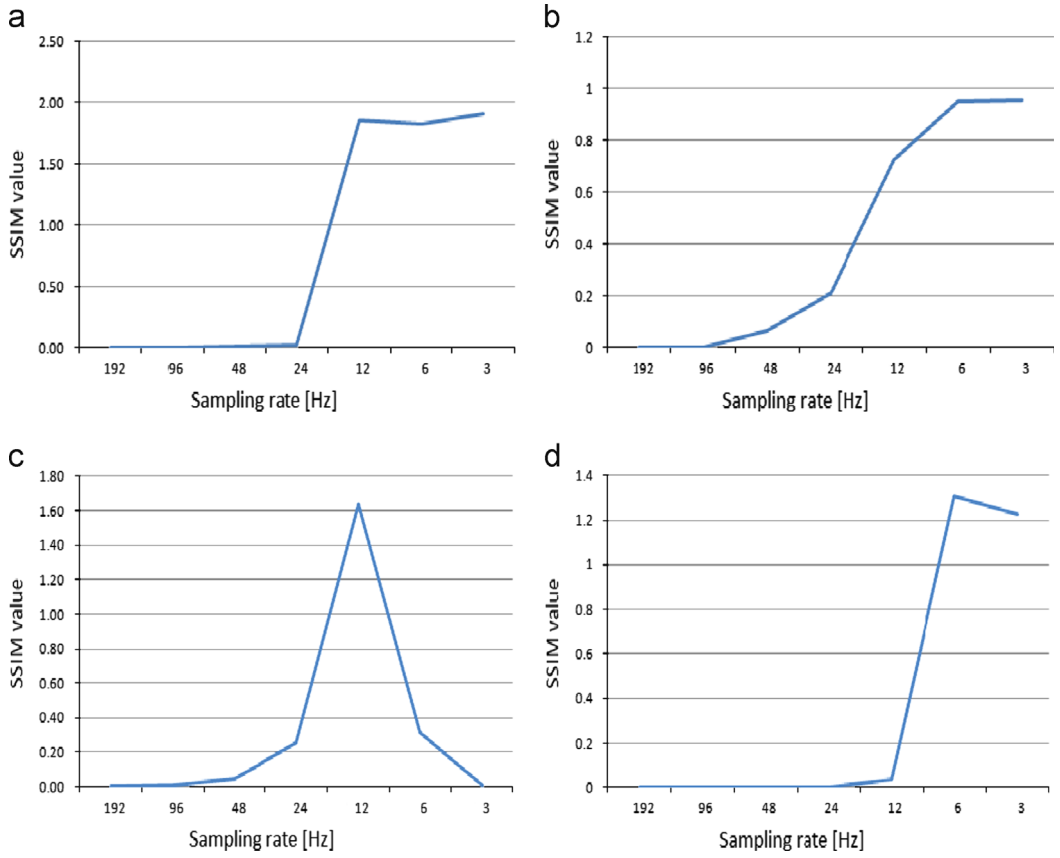

Fig. 5. The error of thermal image with different sampling rate: (a) independent signal image 1, (b) independent signal image 2, (c) independent signal image 3, and (d) independent signal image 4. (Abscissa represents lowering the frequency multiple and vertical coordinate represent the value of SSIM after reducing the frequency in four independent components.)

Table 2
The comparison of estimated ISIs obtained by SCBSS on different sampled IR data.

	The critical sampling rate (Tsc)	The mean of RMSE value (Ts > Tsc)	The variance of RMSE value (Ts > Tsc)	The mean of RMSE value (Ts < Tsc)	The variance of RMSE value (Ts < Tsc)
ISI 1	24	0.0075	0.0065	1.8627	0.037
ISI 2	48	0.0241	0.00094758	0.7105	0.3207
ISI 3	48	0.0184	0.0182	0.5538	0.6356
ISI 4	12	0.0077	0.0149	1.2687	0.0422

Note: Ts means the sampling rate, and Tsc means the critical sampling rate.

From Fig. 5 and Table 2, in order to analyze different performance of high and low end ECPT system for thermal image sequences, four independent signal images which contain all information of thermal images are analyzed. From Fig. 5, a linear relationship with errors and sampling rates does not exist in independent signal image 3. However, there is critical sampling rate in independent signal image 3, this critical sampling rate can distinguish different levels of the error. When the sampling rate is higher than the critical multiple, the difference of the error between each other is not great. When the frequency is lower than the critical frequency, the difference of the error between each other becomes great. ISI 1 which highlights the singular pattern around the crack tips is still consistent with the conclusion as shown in Fig. 3.

From Fig. 5, the four individual components are owing to the different heat transfer process of the location as shown in Fig. 1. This is the reason for the different results of every independent component as shown in Fig. 5. For ISI 1, the mean of SSIM value is 0.0075 and variance gives 0.0065 within the range of 24–192 Hz, the mean of SSIM value is 1.8627 and variance gives 0.0370 within the range of 3 Hz up to 12 Hz. For ISI 2, the mean of SSIM value is 0.0241 and variance gives 9.4758e−004 within the range of 48–192 Hz, the mean of SSIM value is 0.7105 and variance gives 0.3027 within the range of 3–24 Hz. For ISI 3, the mean of SSIM value is 0.0184 and variance gives 0.0182 within the range of 48–192 Hz, the mean of SSIM value is 0.5538 and variance gives 0.6356 within the range of 3–24 Hz. For ISI 4, the mean of SSIM value is 0.0077 and variance gives 0.0149 within the range of 12–192 Hz, the mean of SSIM value is 1.2687 and variance gives 0.0422 within the range of 3–6 Hz.

Therefore, the critical sampling rate which can distinguish different levels of the error, can be found and is similar to Fig. 4. For ISI 1, the critical sampling rate is 24 as shown in Fig. 5(a). For ISI 2 and 3, the critical sampling rate is 48 as shown in Fig. 5 (b) and (c). For ISI 4, the critical sampling rate is 12 as shown in Fig. 5(d). Therefore, in order to ensure the quality of the thermal image sequence as much as possible, the sampling rate should be higher than 48 Hz.

4. Conclusion and future work

Sampling rates influence the estimation accuracy of defect detection and experimental analysis shows that the defect detection on low sampled IR data can induce the error. In this paper, the impact of using SCBSS on the different down sampled IR data is discussed and the conclusion can be drawn as: 1) Within certain sampling rate range from 393 to 24 Hz, the feature extraction results of thermal images on defect region is acceptable with error variance of 0.0065 and the transient responses on defect region can be accurately detected within error variance of 0.138; 2) In order to guarantee the accuracy of the estimation of all thermal as well as their associated transient patterns, sampling rate should be higher than 48 Hz; 3) From our comparison results, the suggestion of the limited sampling rate is 48 Hz by using ECPT system. Therefore the proper choosing of IR sampling rate can not only achieve a sufficient level for defect detection but also reduce the data redundancy and the cost of equipment. Through this comparative experimental study in conjunction with error estimates algorithms, it can be concluded that for defect detection, low sampling frequency in comparison to high-end 383 Hz sampling frequency, can still obtain acceptable performance as long as appropriate signal processing algorithms are used. This conclusion can be used as a basis for select the sampling rate for defect detection and further study focus on expand this method to investigate more kind of materials as well as different size of defect.

Acknowledgements

This work was funded by the National Natural Science Foundation of China (Grant No.51377015) and partially funded by Sichuan Science and Technology Department (Grant No. 2013HH0059), in part by the University of Electronic Science and Technology of China, in part by National Research center of sensors Engineering (Chengdu), inpart by Shenyang Academy of Instrumentation Co. Ltd, in part by Health Monitoring of Offshore Wind Farms (HEMOW), in part by Cognitive-Networks -Enabled Transnational Proactive Healthcare (CoNHealth).

References

[1] Fuentes S Borja, Carmona José L, Bochud, Nicolas, Gomez, Angel M, Peinado, Antonio M. Model-based cepstral analysis for ultrasonic non-destructive evaluation of composites. In: Acoustics, Speech and Signal Processing, ICASSP; March 2012. p. 1713–20.
[2] Jasinien E, Raiutis R, literis R, Voleiis A, Vladiauskas A, Mitchard D, et al. NDT of wind turbine blades using adapted ultrasonic and radiographic techniques. Insight 2009;51(9):477–83.
[3] Ghoshal A, Martin WN, Schulz MJ, Chattopadhyay A, Prosser WH, Kim HS. Geometric optimization of a differential planar eddy currents probe for non-destructive testing. Sens Actuators A—Phys 2013;197:96–105.
[4] Kordatos EZ, Aggelis DG, Matikas TE. Monitoring mechanical damage in structural materials using complimentary NDE techniques based on thermography and acoustic emission. Compos Part B: Eng 2012;43(6):2676–86.
[5] Ghasr MT, Abou-Khousa MA, Kharkovsky S, Zoughi R, Pommerenke D. Portable real-time microwave camera at 24 GHz. IEEE Trans Antennas Propag 2012;60(2):1114–25.
[6] Egbert A. X-ray nanoCT of electronic components: visualizing of internal 3D-structures with submicrometer resolution. In: Electronics System-Integration Technology Conference ESTC; 2008. p. 399–402.
[7] Chai TC, Wongi BS, Bai WM, Trigg A, Lain YK. A novel defect detection technique using active transient thermography for high density package and interconnections. In: Electronic Components and Technology Conference, ECTC; 2003. p. 920–5.
[8] Masashi Ishikawa, Hiroshi Hatta, Yoshio Habuka, Ryo Fukui, Shin Utsunomiya. Detecting deeper defects using pulse phase thermography. Infrared Phys Technol 2013;57(2):42–9.
[9] Peng D, Jones R. Modelling of the lock-in thermography process through finite element method for estimating the rail squat defects. Eng Fail Anal 2013;28:275–88.
[10] Avdelidis NP, Hawtin BC, Almond DP. Transient thermography in the assessment of defects of aircraft composites. NDT&E Int 2003;36:433–9.
[11] Zhi Z, Ning T, Feng L, Zhang C. Specified value based defect depth prediction using pulsed thermography. J Appl Phys 2012;112(2):023112–2-7.
[12] Meola C. Nondestructive evaluation of materials with rear heating lock-in thermography. IEEE Sens J 2007;7(10):1388–9.
[13] Huth S, Breitenstein O, Huber A, Lambert U. Localization of gate oxide integrity defects in silicon metal-oxide-semiconductor structures with lock-in IR thermography. J Appl Phys 2000;88(7):4000–3.
[14] Ghali VS, Jonnalagadda N, Mulaveesala R. Three-dimensional pulse compression for infrared nondestructive testing. IEEE Sens J 2009;9(7):832–3.
[15] Tian Gui Yun, He Yunze, Adewale Ibukun, Simm Anthony. Research on spectral response of pulsed eddy current and NDE applications. Sens Actuators A—Phys 2009;189:313–20.
[16] Li Y, Chen ZM, Qi Y. Generalized analytical expressions of lift off intersection in PEC and a lift off-intersection-based fast inverse model. IEEE Trans Magn 2011;47(10):2931–4.
[17] Wilson J, Tian GY, Abidin IZ, Yang S, Almond D. Modelling and evaluation of eddy current stimulated thermography. Nondestruct Test Eval 2010;25 (3):205–18.
[18] Adewale Ibukun Dapo, Tian Gui Yun. Decoupling the influence of permeability and conductivity in pulsed eddy current measurements. IEEE Trans Magn 2013;49(3):1119–27.
[19] Ganesan NBN, Krishnamurthy CV, Balasubramaniam K. Simultaneous estimation of electrical and thermal properties of isotropic material from the Tone-Burst Eddy Current Thermography (TBET) time–temperature data. IEEE Trans Magn 2011;47:2213–9.
[20] Yin Aijun, Gao Bin, Tian Gui Yun, Woo WL, Li Kongjing. Physical interpretation and separation of eddy current pulsed thermography. J Appl Phys 2013;113(6).
[21] Wilson J, Tian GY, Abidin IZ, Yang Suixian, Almond D. Plused eddy current thermography: system development and evaluation. Insight—Non-destruct Test Cond Monit 2010;52(2):87–90.
[22] Almond DP, Weeks B, Li T, Pickering SG, Koston E, Wilson J, et al. Thermographic techniques for the detection of cracks in metallic components. Insight —Non-destruct Test Cond Monit 2011;53(11):614–20.
[23] Zenzinger G, Bamberg J, Satzger W, Carl V. Thermographic crack detection by eddy current excitation. Nondestruct Test Eval 2007;22(2–3):101–11.

[24] Weekes B, Almond DP, Gawley P, Barden T. Eddy-current induced thermography-probability of detection study of small fatigue cracks in steel, titanium and nickel-based superalloy. NDT&E Int 2012;49:47–56.
[25] Wilson J, Tian G Y, Mukriz I, Almond D. PEC thermography for imaging multiple cracks from rolling contact fatigue. NDT&E Int 2011;44:505–12.
[26] Abidin IZ, Tian GY, Wilson J, Yang S, Almond D. Quantitative evaluation of angular defects by pulsed eddy current thermography. NDT&E Int 2010;43 (7):537–46.
[27] Yang SX, Tian GY, Abidin IZ, Wilson J. Simulation of edge cracks using pulsed eddy current stimulated thermography. J Dyn Syst Meas Control 2011:011008.1–6.
[28] Oswald-Tranta, B, Wally, G. Thermo-inductive surface crack detection in metallic materials. In: Proceedings of the 9th European Conference on NDT. Berlin; 2006.
[29] Vrana J, Goldammer M, Baumann J, Rothenfusser M, Arnold W. Mechanisms and models for crack detection with induction thermography. Rev Prog Quant Nondestruct Eval 2008;27:475–82.
[30] Khan AA, Vrabie V, Mars JI, Girard A, D'Urso G. A source separation technique for processing of thermometric data from fiber-optic DTS measurement for water leakage identification in dikes. IEEE Sens J 2008;8(7):1118–29.
[31] Rajic N. Principal component thermography for flaw contrast enhancement and flaw depth characterisation in composite structures. Compos Struct 2002;58:521–8.
[32] Bai Libing, Gao Bin, Tian Gui Yun, Woo WL, Cheng Yuhua. Spatial and time patterns extraction of eddy current pulsed thermography using blind source separation. IEEE Sens J 2013;13(6):2094–101.
[33] Bruckstein AM, Elad M, Kimmel R. Down scaling for better transform compression. IEEE Trans Image Process 2003;12(9):1132–44.
[34] Bouzid OM, Tian GY, Neasham J, Sharif. B. Investigation of sampling frequency requirements for acoustic source localisation using wireless sensor networks. Appl Acoust 2013;74(2):269–74.
[35] Cheng L, Tian Gui Yun. Surface crack detection for carbon fiber reinforced plastic (CFRP) materials using pulsed eddy current thermography. IEEE Sens J 2011;11:3261–8.
[36] Yao-Ze Feng, Da-Wen Sun. Near-infrared hyperspectral imaging in tandem with partial least squares regression and genetic algorithm for non-destructive determination and visualization of Pseudomonas loads in chicken fillets. Talanta 2013;109:74–83.
[37] Wang Z, Bovik AC, Sheikh HR, Simoncelli EP. Image quality assessment: from error visibility to structural similarity. IEEE Trans Image Process 2004;13 (4):600–12.
[38] Farzana E, Tanzid M, Mohsin KM, Bhuiyan MIH. Bilateral filtering with adaptation to phase coherence and noise. Signal Image Video Process 2013;7(2):367–76.
[39] Gao Bin, Woo WL, Dlay SS, Single channel source separation using EMD-subband variable regularized sparse features. IEEE Trans Audio, Speech Lang Process. 2011;19:916–76.